Acta Oceanol. Sin., 2021, Vol. 40, No. 5, P. 80–93
https://doi.org/10.1007/s13131-021-1729-y
http://www.hyxb.org.cn
E-mail: ocean2@hyxb.org.cn

Short-term offshore extension of Brahmaputra-Ganges and Irrawaddy freshwater plumes to the central northern Bay of Bengal based on *in situ* and satellite observations

Zhiyuan Li[1, 2], Saihua Huang[1], Xiaohua Zhu[2, 3, 4*], Zhilin Sun[5], Yu Long[2], Huawei Xie[1]

[1] Key Laboratory for Technology in Rural Water Management of Zhejiang Province, Zhejiang University of Water Resources and Electric Power, Hangzhou 310018, China

[2] State Key Laboratory of Satellite Ocean Environment Dynamics, Second Institute of Oceanography, Ministry of Natural Resources, Hangzhou 310012, China

[3] School of Oceanography, Shanghai Jiao Tong University, Shanghai 200030, China

[4] Southern Marine Science and Engineering Guangdong Laboratory (Zhuhai), Zhuhai 519080, China

[5] Ocean College, Zhejiang University, Zhoushan 316021, China

Received 2 April 2020; accepted 3 July 2020

Abstract

In this study, the short-term offshore extension of Brahmaputra-Ganges (BG) and Irrawaddy freshwater plumes to the central northern Bay of Bengal (BoB) was investigated based on *in situ* and satellite observations. In the summer and winter of 2015, two significant freshening events with periods of weeks were observed from a moored buoy at 15°N, 90°E in the BoB. Soil Moisture Active Passive (SMAP) satellite sea surface salinity compares well with the *in situ* data and shows that these freshening events are directly related to the short-term offshore extension of the BG and Irrawaddy freshwater, respectively. These data combined with the altimeter sea level anomaly data show that the offshore extending plumes result from freshwater modulated by eddies. During summer, the BG freshwater is modulated by a combination of three closely located eddies: a large anticyclonic eddy (ACE) off the northwestern BoB coast and two cyclonic eddies in the northern BoB. Consequently, the freshwater extends offshore from the river mouth and forms a long and narrow tongue-shaped plume extending southwestward to the central BoB. During winter, the Irrawaddy freshwater is modulated by two continuous ACEs evolved from Rossby wave propagating westward from the Irrawaddy Delta off Myanmar, forming a tongue-shaped plume extending to the central BoB. Strong salinity fronts are formed along the boundaries of these tongue-shaped plumes. These findings confirm good capability of the SMAP data to investigate the short-term offshore extension of the BG and Irrawaddy freshwater. This study provides direct evidences of the pathways of the offshore extension of the BG and Irrawaddy freshwater and highlights the role of eddies in the northern BoB freshwater plume variability.

Key words: freshwater plume, Bay of Bengal, freshening event, SMAP, Brahmaputra-Ganges and Irrawaddy, cyclonic and anticyclonic eddies

Citation: Li Zhiyuan, Huang Saihua, Zhu Xiaohua, Sun Zhilin, Long Yu, Xie Huawei. 2021. Short-term offshore extension of Brahmaputra-Ganges and Irrawaddy freshwater plumes to the central northern Bay of Bengal based on *in situ* and satellite observations. Acta Oceanologica Sinica, 40(5): 80–93, doi: 10.1007/s13131-021-1729-y

1 Introduction

The northern Indian Ocean (NIO) is composed of two semi-enclosed basins: the Arabian Sea (AS) in the west and the Bay of Bengal (BoB) in the east. The annual mean sea surface salinity (SSS) distributions in the AS and BoB show distinct features, with higher SSS in the AS and lower SSS in the BoB (Fig. 1a) (Han and McCreary, 2001; Li et al., 2016; Sun et al., 2019). This difference is because the AS features higher evaporation and lower precipitation and receives high salinity water from both the Red Sea and Persian Gulf (Rao and Sivakumar, 2003; Xi et al., 2015; Li et al., 2018). In contrast, the BoB is dominated by much higher precipitation, relatively lower evaporation and receives substantial amounts of freshwater from several major rivers (Sengupta et al., 2006; Zhou and Murtugudde, 2014; Li et al., 2017b), for example, the Brahmaputra-Ganges (BG) River and Irrawaddy River are among the world's 50 largest rivers, and the annual discharge is approximately 4.0×10^4 m^3/s (Sengupta et al., 2006; Dai et al., 2009; Papa et al., 2010, 2012) (Fig. 1b). The discharge of the BG River and Irrawaddy River increase in July and reach a maximum value in August or September (Dai et al., 2009) (Fig. 1c). The sub-

Foundation item: The National Natural Science Foundation of China under contract Nos 41920104006 and 41776107; the Key Program of the National Natural Science Foundation of China under contract No. 91647209; the Key Special Program on the Science and Technology of Zhejiang Province under contract No. 2015C03015; the Scientific Research Fund of SIO under contract Nos JZ2001 and JT1801; the Scientific Research Fund of the State Key Laboratory of Satellite Ocean Environment Dynamics, SIO under contract No. SOEDZZ2106; the Open Fund of State Key Laboratory of Satellite Ocean Environment Dynamics, Second Institute of Oceanography, MNR under contract No. QNHX2114.

*Corresponding author, E-mail: xhzhu@sio.org.cn

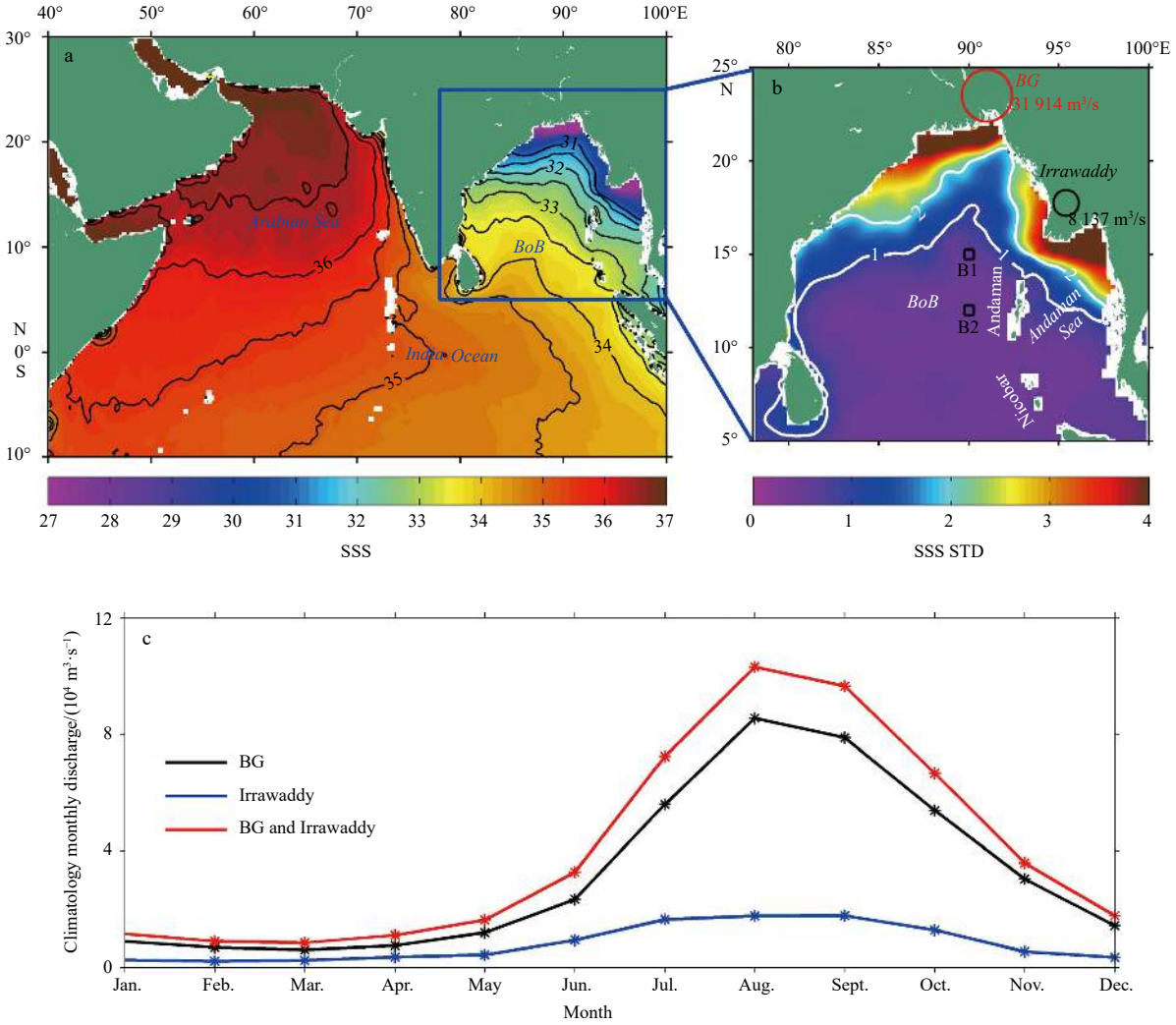

Fig. 1. Annual mean Soil Moisture Active Passive (SMAP) sea surface salinity (SSS) in the northern India Ocean (NIO) (a) and standard deviation (STD) of daily SMAP SSS in the Bay of Bengal (BoB) (b). The SMAP data are from April 2015 to December 2018. The circles indicate the locations of the Brahmaputra-Ganges (BG) River and Irrawaddy River, and the annual mean discharges are labeled in the panel. For each river, the size of the circle is proportional to the magnitude of the annual mean discharge. The two black squares represent the RAMA buoy stations at B1 (15°N, 90°E) and B2 (12°N, 90°E). Climatological monthly discharge of the BG River and Irrawaddy River and the summation of the two rivers (c).

stantial freshwater input from the BG River and Irrawaddy River leads to low salinity in the surface layer and causes a strong near surface stratification (Shetye et al., 1996; Sengupta et al., 2006; Thadathil et al., 2007, 2016; Liu et al., 2018). The strong saline stratification in the surface layer favors the formation of a barrier layer that profoundly influences the air-sea interaction in the BoB (Sprintall and Tomczak, 1992; Han et al., 2001; Du et al., 2009; Liu et al., 2011; Qiu et al., 2012; Thangaprakash et al., 2016).

In addition to the low salinity feature, the BoB is also characterized by large SSS variability, especially in the northern area (Fig. 1b). Two distinctive zones with large SSS variability are clearly visible along two sides of the BoB, reflecting the extension of the BG freshwater and Irrawaddy freshwater. On the western side, the standard deviation (STD) of SSS is large at the BG River Mouth and decreases southward along the coast with relatively large values (>1) extending to the area south of Sri Lanka. These features reflect the movement of the BG freshwater, which was previously found in hydrographic observations (Shetye et al., 1991; Murty et al., 1992; Shetye et al., 1996). Recently, Chaitanya et al. (2014) observed a narrow strip of freshwater with very low salinity ("river in the sea") along the western BoB coast based on salinity measurements collected by fishermen. Chaitanya et al. (2014) showed that the "river in the sea" extends southward along the coast due to the advection of the BG freshwater by the East India Coastal Current (EICC). The extension of the BG freshwater in the BoB was further studied by numerical models (Akhil et al., 2014, 2016; Benshila et al., 2014) and satellite observations (Sengupta et al., 2016; Fournier et al., 2017; Sree Lekha et al., 2018). From the satellite SSS and altimeter sea level anomaly (SLA), Sengupta et al. (2016) discussed the pathway of the BG freshwater in the BoB and concluded that the freshwater is transported by the basin circulation and modulated by eddies. Along the eastern side, the STD of SSS is notably comparable to that along the western side, and its value is large at the Irrawaddy River Mouth and decreases both northward and southward along the coast. The large STD of SSS along the eastern side strongly suggests a remarkable extension of the Irrawaddy freshwater. However, the extension of the Irrawaddy freshwater has been

poorly studied because of the extremely sparse *in situ* observations in the eastern BoB (Chatterjee et al., 2012; Akhil et al., 2014; Liu et al., 2018; Ashin et al., 2019).

Freshening events were often observed from Argo floats and moored buoys in the BoB. Parampil et al. (2010) observed the occurrence of prominent freshening in the near surface salinity from Argo floats in the central BoB. The researchers showed that freshening is independent of local freshwater flux but is due to the advection of river freshwater by eddies or filaments. Rao et al. (2011) identified significant freshening events in the summer and winter of 2009 from an Argo float at 19°N, 89°E and a moored buoy at 15°N, 90°E (B1, black square in Fig. 1b). The researchers indicated that the offshore extension of the BG freshwater is responsible for the observed summer freshening events. Based on the moored salinity at 18°N, 89.5°E, Sengupta et al. (2016) observed two freshening pulses in the summer and winter of 2013. The researchers proposed that the summer freshening pulse comes from the BG freshwater and that the winter freshening pulse comes from the Irrawaddy freshwater. Sree Lekha et al. (2018) found that during the freshening event observed in the summer of 2013, the near surface salinity between two closely located mooring stations shows a large lateral difference, indicating that the river freshwater extends offshore to the central northern BoB as a narrow filament. These studies confirmed the occurrences of short-term freshening events in the central northern BoB in both summer and winter. However, due to the limited spatial coverage of the *in situ* observational data, the processes related to the short-term freshening events (especially the winter freshening) are still unclear and remain a speculation. To better investigate the short-term freshening processes, satellite observations with high spatial-temporal resolution are needed.

Launched on January 31, 2015, NASA's Soil Moisture Active Passive (SMAP) satellite provides a better SSS retrieval compared with other satellite observations, especially in coastal regions (Fore et al., 2016; Tang et al., 2017; Bao et al., 2019; Hackert et al., 2019). The SMAP satellite data have been successfully used to study river plumes (Fournier et al., 2016, 2017; da Silva and Castelao, 2018). da Silva and Castelao (2018) used the SMAP SSS to study the Mississippi River plume variability and demonstrated that the SMAP data are able to characterize plume fronts and filaments in estuary regions. In the summer and winter of 2015, two significant freshening events with periods of weeks were observed from a moored buoy at 15°N, 90°E. By combining the moored buoy and SMAP satellite data, the present study aims to interpret the short-term freshening events observed in the central northern BoB and to further investigate the offshore extension of the BG and Irrawaddy freshwater. This paper is organized as follows. In Section 2, the data and method used in this study are described, and the SMAP data are validated. In Section 3, the two freshening events with periods of weeks are shown from the *in situ* observations. The short-term offshore extension of the BG and Irrawaddy freshwater is revealed from the SMAP SSS, and modulation of these freshwater by eddies is shown from the altimeter data. A discussion is provided in Section 4, which is followed by a summary in Section 5.

2 Data and methods

2.1 *Satellite SSS*

The SMAP SSS is the L3 V4.2 dataset produced by NASA's Jet Propulsion Laboratory (Fore et al., 2016). The SMAP SSS data have a spatial resolution of 0.25° and an 8-day running mean time window and are available from April 2015 to December 2018. The data are downloaded from the Asia-Pacific Data-Research Center of the International Pacific Research Center (IPRC) at the University of Hawaii (http://apdrc.soest.hawaii.edu).

The Soil Moisture and Ocean Salinity (SMOS) L3 data are provided by the Barcelona Expert Center (BEC) in Spain (http://bec.icm.csic.es/). The BEC provides two objectively analyzed products: monthly binned SSS data with a spatial resolution of 1° and 9-day running mean SSS data with a spatial resolution of 0.25°. Both products are available from January 2011 to December 2016. The 9-day running mean data are used because of its finer spatial resolution.

The Aquarius SSS V5.0 data with a spatial resolution of 1° are distributed by NASA's Physical Oceanography Distributed Active Archive Center. These data are the latest version of the salinity data produced by the Aquarius project (Le Vine et al., 2018). Based on estimates from the Aquarius SSS, the IPRC produced an optimal interpolation of SSS (OISSS) to correct SSS retrievals for large-scale satellite biases (Melnichenko et al., 2014). The IPRC monthly 0.5°×0.5° global gridded OISSS V5.0 data are available from August 2011 to May 2015 (http://apdrc.soest.hawaii.edu).

2.2 *In situ SSS*

The climatological monthly World Ocean Atlas 2018 (WOA18) objective analyzed salinity field with a spatial resolution of 0.25° is used and these data are available at the National Centers for Environmental Information (https://www.nodc.noaa.gov/).

The monthly, global salinity gridded Argo dataset (Hosoda et al., 2008) which is based on the Grid Point Value of the Monthly Objective Analysis using Argo float data (MOAA GPV) are used. This Argo product combines data from Argo floats, Triangle Trans-Ocean Buoy Network and available conductivity-temperature-depth casts. The MOAA GPV dataset has a spatial resolution of 1° and is available from January 2001 to December 2018 on the Argo website of the Japan Agency for Marine-Earth Science and Technology (http://www.jamstec.go.jp). The Argo data (upper 150 m) are vertically linearly interpolated into 1 m intervals for estimating the mixed layer depth (MLD). The MLD is estimated based on a variable density criterion (Kara et al., 2000) as follows:

$$\Delta\sigma = \sigma_t\left(T_0 - \Delta T, S_0, P_0\right) - \sigma_t\left(T_0, S_0, P_0\right), \tag{1}$$

where $\Delta\sigma$ is the density difference from the surface to the base of the MLD and T_0, S_0 and P_0 are the surface values of temperature, salinity and pressure, respectively. σ_t is the surface density (kg/m^3). The MLD is defined as the depth at which the density increase $\Delta\sigma$ from the surface value is equal to the temperature decrease by ΔT (0.5°C) (Felton et al., 2014; Girishkumar et al., 2017; Li et al., 2017a). The isothermal layer depth (ILD) is defined as the depth at which the surface temperature decreases by 0.5°C. The barrier layer thickness (BLT) is the positive difference between the ILD and MLD.

2.3 *Moored buoy*

Daily salinity and temperature data measured by the Research Moored Array for African-Asian-Australian Monsoon Analysis and Prediction (RAMA) (McPhaden et al., 2009) at two stations B1 (15°N, 90°E) and B2 (12°N, 90°E) in the central northern BoB are used. The RAMA data are provided by the Global Tropical Moored Buoy Array Project Office of the National Oceanic and Atmosphere Administration and the Pacific Marine Environmental Laboratory (https://www.pmel.noaa.gov/). The RAMA data are vertically linearly interpolated into 1 m intervals for analysis.

2.4 *Auxiliary data*

The ocean surface current analysis real-time(OSCAR) near surface current is generated by Earth Space Research (https://www.esr.org/research/oscar/). The OSCAR near-surface ocean current is derived using quasi-linear and steady flow momentum equations (Bonjean and Lagerloef, 2002). The horizontal velocity is directly estimated from sea surface height, surface vector wind and sea surface temperature. The OSCAR surface current has a spatial resolution of (1/3)° with 5-day resolution, and the data are available from 1992 to present.

The daily maps of SLA with a spatial resolution of 0.25° are obtained from the Copernicus Marine and Environment Monitoring Service (CMEMS, http://marine.copernicus.eu/). The SLA is an anomaly with respect to the mean from 1993 to 2012. The same maps were previously distributed by the Archiving, Validation and Interpretation of Satellite Oceanographic data service. The CMEMS gridded data produced using all satellite altimeter measurements are used, which are available from 1993 to present.

2.5 *SMAP SSS validation*

Since the data became available in April 2015, the SMAP SSS has been validated by many investigators (Fore et al., 2016; Tang et al., 2017; Bao et al., 2019; Hackert et al., 2019). Bao et al. (2019) comprehensively compared the SMAP data with *in situ* observations and SMOS and Aquarius satellite products. The comparison shows good agreement between the SMAP SSS and other SSS data. The SMAP data were also widely used to study SSS variability, and the data show good performance, especially in characterizing the river plume variability (Fournier et al., 2016, 2017; da Silva and Castelao, 2018). In this study, the SMAP SSS is briefly validated with *in situ* and other satellite SSS products. Figure 2 shows the climatology annual mean SSS for the WOA18, Argo, SMOS and Aquarius data. The WOA18 and Argo SSS were obtained from the respective surface salinity field. All four SSS datasets show very similar spatial distributions with the SMAP SSS, although slight differences between SMAP SSS and other SSS data are also noted. For example, the Argo and Aquarius SSS are smoother in space, possibly due to the relatively coarse spatial resolution of the data. Compared with the WOA18 and SMOS SSS, the SMAP SSS is higher in the northern AS and lower in the river mouths of the BoB. Overall, in spite of these regionally small differences, the SMAP SSS shows good agreement with the WOA18, Argo, SMOS and Aquarius SSS products.

3 Results

3.1 *Two freshening events observed from RAMA buoy salinity*

Figure 3 shows the temporal evolution of depth-dependent RAMA buoy salinity at B1 (15°N, 90°E) and B2 (12°N, 90°E) from April 2015 to March 2016 (one complete annual cycle). At Station B1 (Fig. 3a), the RAMA salinity shows that a freshening event (event 2) on timescales of weeks is very remarkable from December 2015 to January 2016. In August 2015, another freshening event (event 1) also occurred. Although this freshening event is not as striking from the salinity in the whole water column, this freshening event is clearly identified from the near surface salinity, as shown below. At Station B2 (Fig. 3b), the RAMA salinity is much higher than that at Station B1 for almost the whole period. Moreover, the salinity is high during the two freshening events shown from Station B1. This indicates that the freshwater plumes do not spread as far as south of 12°N. Therefore, the two freshen-

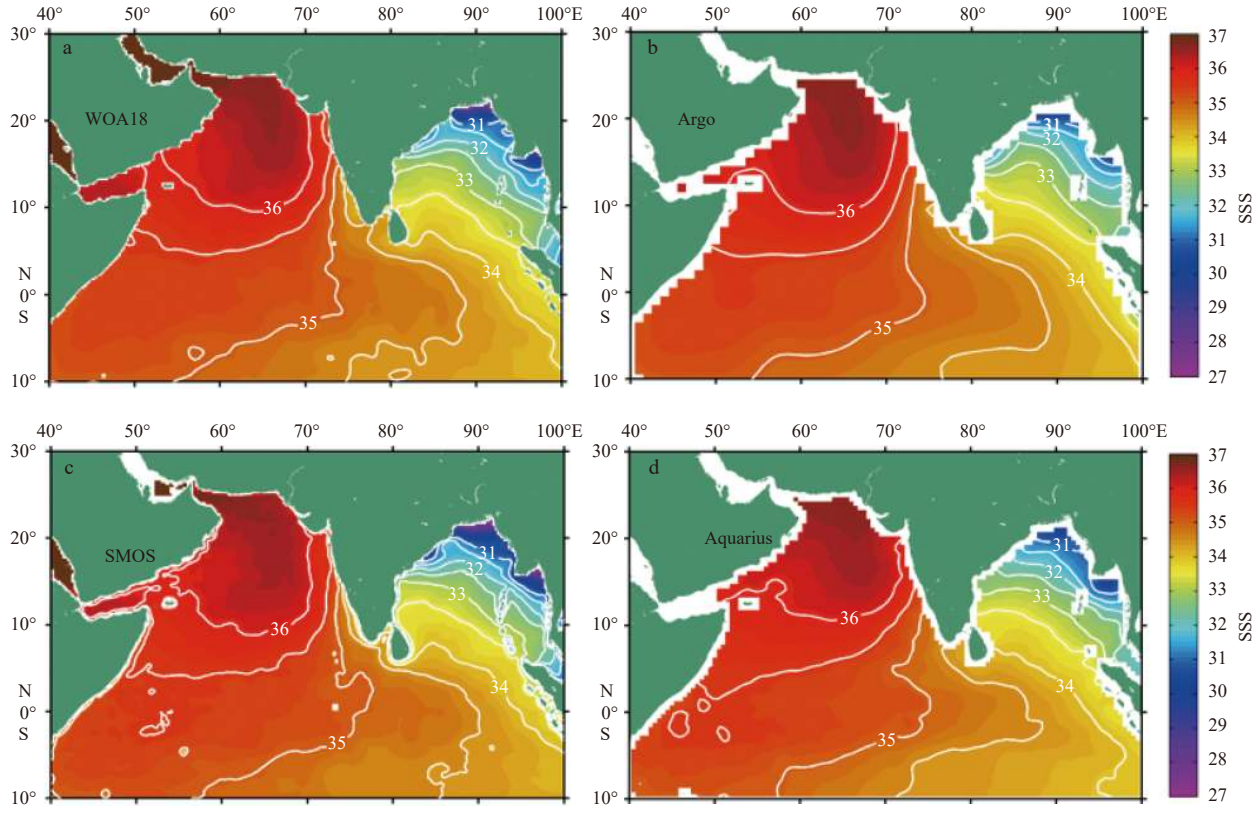

Fig. 2. Climatological annual mean of sea surface salinity (SSS) for WOA18 (a), Argo (b), SMOS (c) and Aquarius (d) in the NIO. The white lines indicate the SSS contours with an interval of 0.5.

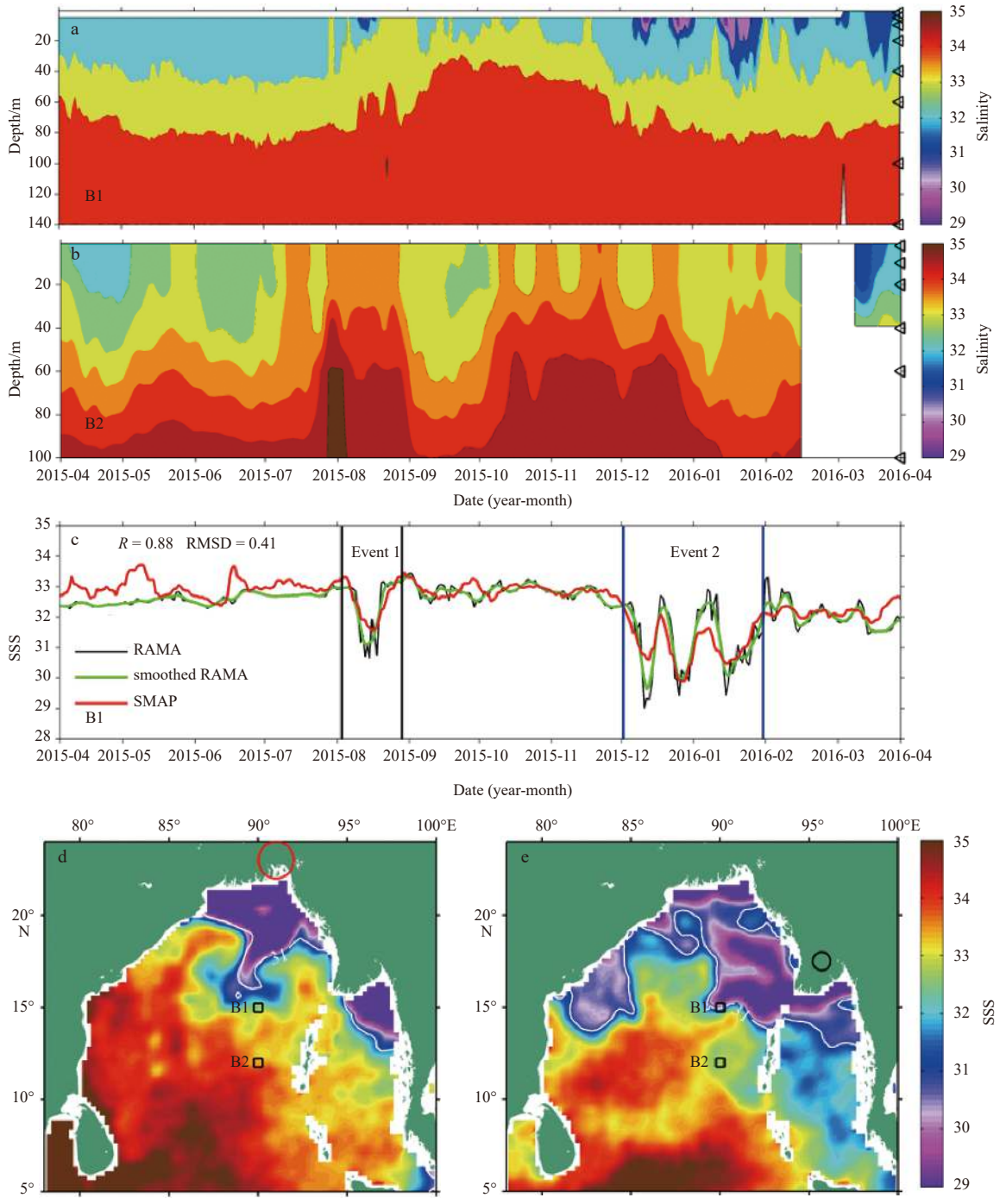

Fig. 3. Temporal evolution of daily salinity measured by the RAMA buoy at Stations B1 (a) and B2 (b) from April 2015 to March 2016 (the black triangles denote the depths of measurement sensors); time series of the daily original (black line) and 8-day smoothed (green line) RAMA and SMAP (red line) SSS at Station B1 (c); and representative SMAP SSS snapshot on August 9, 2015 (Event 1) (d) and December 28, 2015 (Event 2) (e) during the two freshening events (the white line indicates the 31 SSS contour, and the black squares indicate the RAMA buoy at Stations B1 and B2).

ing events are investigated by using the RAMA salinity at Station B1 in the following.

Because the RAMA salinity (Station B1) at the 1 m level is not available for the whole period, the salinity at 5 m is nominally considered as that from the sea surface. Now, the freshening event in August is clearly distinguished from the RAMA SSS (black line in Fig. 3c). In the freshening event 1, the RAMA SSS drops sharply within ten days. In the freshening event 2, periodic decreases and restorations in SSS are very noticeable over a period of weeks. It is noted that the winter freshening has a deeper depth (30–40 m) than the summer freshening (10 m). Freshening events in summer and winter were also previously observed by Rao et al. (2011) and Sengupta et al. (2016). The SMAP SSS well captures the two observed freshening events, although the freshening is underestimated from the SMAP SSS (red lines in Fig. 3c). To quantitatively make a comparison with the SMAP

SSS, the RAMA SSS is smoothed at an 8-day running mean time window (green line in Fig. 3c). The time series of the smoothed RAMA and SMAP SSS show good agreement, particularly during the two freshening events. The correlation coefficient between the two time series is 0.88, and the root mean square difference is 0.41. This good agreement encourages us to use the SMAP SSS to interpret the freshening in the central northern BoB and to further investigate the short-term offshore extension of the BG and Irrawaddy freshwater.

During each freshening event, one representative SMAP SSS snapshot is selected to provide the first insight into the freshening in the BoB. On August 9, 2015, the SMAP SSS shows that the BG freshwater extends offshore from the river mouth and forms a tongue-shaped plume extending southwestward to regions near the moored Station B1 (Fig. 3d). On December 28, 2015, the Irrawaddy freshwater extends westward from the Irrawaddy Delta off Myanmar (IDM) and forms a tongue-shaped plume extending to the moored Station B1 (Fig. 3e).

3.2 *Monthly evolution of the freshwater plume and surface current*

Before to investigate the offshore extension of the BG and Irrawaddy freshwater on short-term timescales of weeks, the monthly evolution of the salinity field between April 2015 and March 2016 is shown (Fig. 4). A sudden surge of freshwater occurs at the BG and Irrawaddy river mouths in July 2015 (Fig. 4d), corresponding to the river discharge increase in the summer monsoon (Fig. 1c). However, in the following August, the BG freshwater does not spread southward along the western BoB coast. The freshwater withdraws to the north and extends directly offshore from the river mouth, forming a tongue-shaped plume extending to the central northern BoB (Fig. 4e). In September, this tongue-shaped plume weakens, and the BG freshwater begins to spread rapidly along the western BoB coast. From October to November, the BG and Irrawaddy freshwater spreads along the two sides of the BoB, and the BG freshwater can extend to the south of Sri Lanka (Fig. 4h). In December, a tongue-shaped plume extending westward to the central northern BoB is also noted, indicating the offshore extension of the Irrawaddy freshwater. The BG freshwater decays beginning in December 2015, and the freshwater is very weak and even disappears in February 2016. However, the Irrawaddy freshwater persists until March 2016.

Previous studies reported that the freshwater in the BoB is transported by the basin circulation and modulated by eddies (Akhil et al., 2014; Sengupta et al., 2016; Fournier et al., 2017; Sree Lekha et al., 2018). The OSCAR surface current in the BoB (arrows in Fig. 4) shows numerous cyclonic eddies (CEs) and anticyclonic eddies (ACEs), especially in the western area. These CEs and ACEs have been reported in previous studies (Babu et al., 1991; Chen et al., 2012; Cheng et al., 2013, 2018; Arunraj et al., 2018; Das et al., 2019). Another prominent feature is the seasonally reversing EICC along the western boundary of the BoB. The EICC is northward along the western boundary from April to July and reverses to southward from November to December. From February to March of the next year, the EICC reverses to northward again. In the remaining months, the well-organized EICC is absent. Particularly, from August to October, the flow in the western BoB is characterized by CEs and ACEs. These features are consistent with the findings of McCreary et al. (1993) and Das at al. (2019) that the EICC is disorganized in the presence of various CEs and ACEs during the summer monsoon. The modulation of the freshwater by the EICC and eddies is evident from these monthly maps. For example, the EICC transports freshwater southward along the western BoB coast from November to December (Figs 4h and i). The modulation of freshwater by eddies is more complex and will be illustrated later.

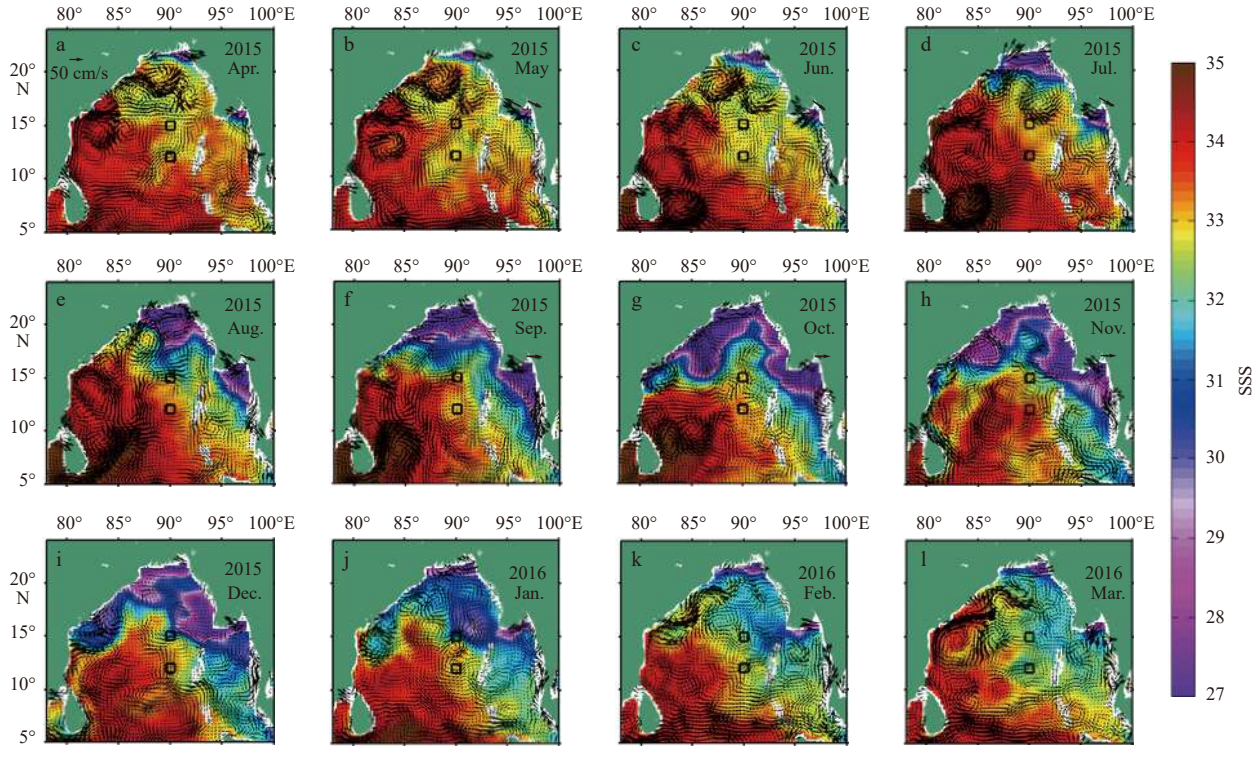

Fig. 4. Monthly evolution of SMAP SSS (color) and OSCAR surface current (arrows) from April 2015 to March 2016.

3.3 *Short-term offshore extension of the BG and Irrawaddy freshwater*

Attention is paid to the periods from August to September 2015 and from December 2015 to January 2016 when the offshore extension of the BG and Irrawaddy freshwater is significant (Figs 3 and 4). The spatial and temporal evolutions of the SMAP SSS during the two periods are shown in Figs 5 and 6. On 1 August, the BG freshwater is distributed at the river mouth in the northernmost BoB (Fig. 5a). In the following ten days, the freshwater extends offshore from the river mouth to the central north-

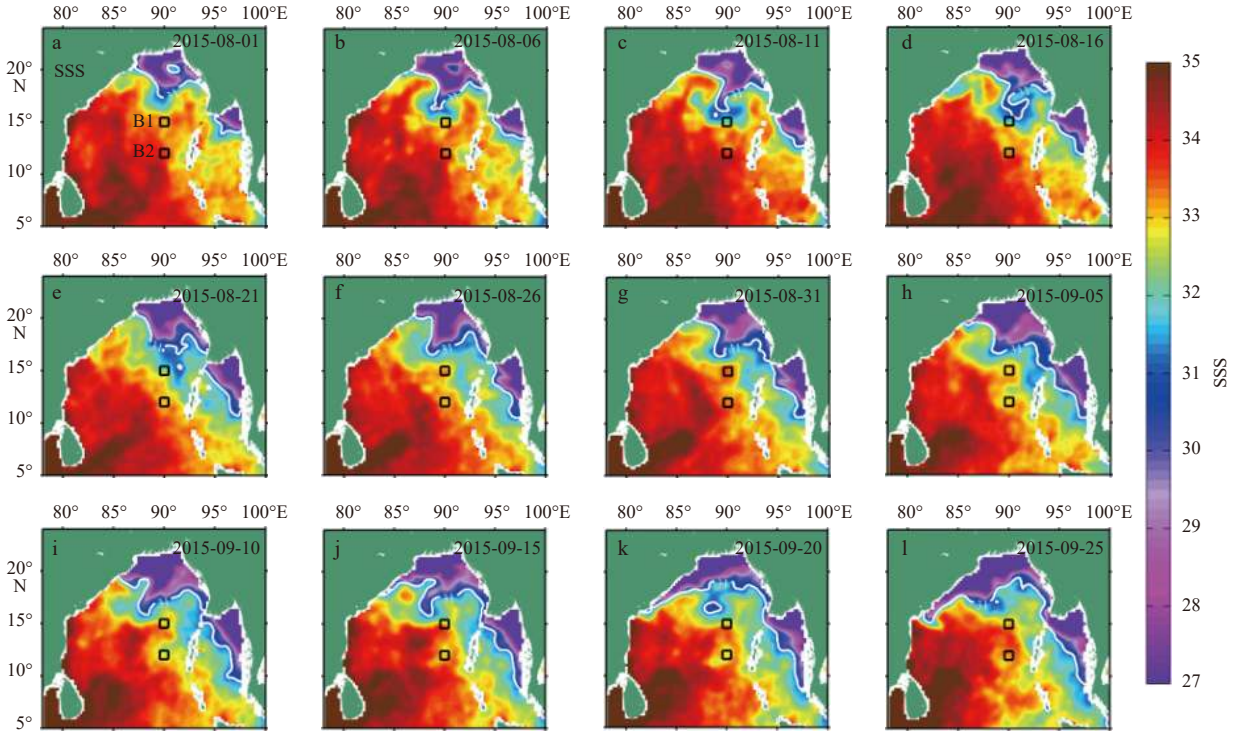

Fig. 5. Offshore extension of the BG freshwater from August to September 2015. The white line indicates the 31 SSS contour.

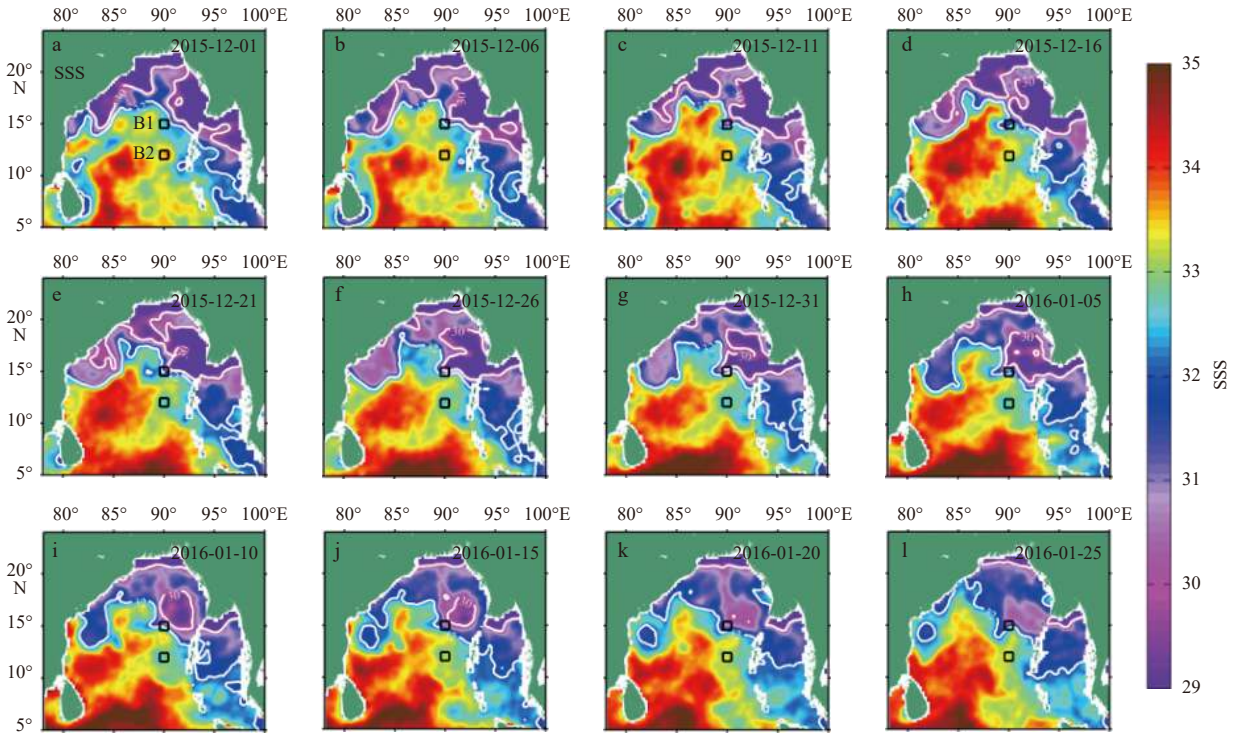

Fig. 6. Offshore extension of the Irrawaddy freshwater from December 2015 to January 2016. The white line indicates the SSS contours of 30 and 32.

ern BoB and forms a clear tongue-shaped plume (Figs 5b and c). The tongue shape of the plume can be approximately represented by the 31 SSS contour extending southwestward to the nearby region at Station B1 (15°N, 90°E). In the middle of August, the BG freshwater plume moves northeastward, and the tongue shape of the plume becomes obscure for one week (Figs 5d and e). Then, the tongue shape becomes clear again and persists until mid-September (Figs 5f–j). After mid-September, the BG freshwater spreads southward along the western BoB coast, and the tongue-shaped plume in the central northern BoB disappears.

The extension of the Irrawaddy freshwater is remarkable from December 2015 to January 2016 (Fig. 6). During the first half of December, the Irrawaddy freshwater extends westward from the IDM into the BoB (Figs 6a–d). When reaching the bump of the IDM, a part of the Irrawaddy freshwater extends northward along the eastern BoB coast. The rest of the freshwater extends westward to the central northern BoB and forms a tongue-shaped plume. As this freshwater extends farther offshore in the central BoB, the low salinity water can detach from the tongue-shaped plume (Fig. 6e). Two branches of the Irrawaddy freshwater extending offshore to the central BoB are identified (Figs 6f and g). In January 2016, the two branches of freshwater merge together and form a large freshwater mass extending offshore to the central BoB (Figs 6h–j). In late January, the offshore extension of the freshwater mass gradually weakens (Figs 6k and l).

The SMAP SSS shows that the BG and Irrawaddy freshwater extends offshore to the central northern BoB, where the ambient water is much saltier. This enables the formation of plume fronts along the boundaries between the freshwater and salty water. To quantitatively estimate the plume fronts, the SSS gradient was calculated. Plume fronts are identified by defining a criterion that the SSS gradient is larger than 0.02 per kilometer, which recognizes tongue-shaped fronts along the boundaries of the BG and Irrawaddy freshwater plumes. Figure 7 shows the BG plume front in summer and the Irrawaddy plume front in winter. In summer, the tongue-shaped BG plume front is approximately bounded by the 31 SSS contour. The plume front extends southwestward to the central northern BoB with a length of the tongue shape of approximately 400 km (Fig. 7a). In winter, the Irrawaddy plume front is approximately bounded by the 30 SSS contour. Correspondingly, two branches of the plume front are noted. In particular, long plume fronts extend from the IDM to the central northern BoB and form a tongue shape in the central BoB.

3.4 *Eddy's role in the short-term plume variability*

The August monthly SMAP SSS and OSCAR surface current maps clearly suggest modulation of the BG freshwater by eddies. However, from the December to January monthly SMAP SSS and OSCAR surface current maps, modulation of the Irrawaddy freshwater by eddies is not very striking. To better characterize these eddies, the SLA and associated geostrophic current from the CMEMS averaged over half a month are shown. In the first half of August 2015 (Fig. 8a), the SLA maps clearly show three eddies close to each other in the northern BoB: a large ACE off the northwestern BoB coast and two CEs (CE1 in the north and CE2 in the south) in the northern BoB. Half a month later (Fig. 8b), the three eddies can still be identified. However, their positions and shapes change, indicating a southwestward propagation. It is found that the tongue-shaped BG plume is the result of freshwater modulated by a combination of these three eddies. Now, how these three eddies modulate the BG freshwater to extend offshore and form the tongue-shaped plume is interpreted. The CE1 is very close to the BG river mouth and carries freshwater southward along the western BoB coast. However, the large ACE off the northwestern BoB coast prohibits the BG freshwater from spreading southward along the western BoB coast. As a result of the combined modulation of CE1 and ACE, the freshwater spreads southeastward to the central northern BoB along the junction of the two eddies. In the central northern BoB, CE2 prohibits freshwater from further spreading southeastward. Moreover, the combined modulation of CE2 and ACE carries freshwater southwestward along the junction of these two eddies. In the central northern BoB, the CE2 modulates the freshwater to first spread eastward and then spread northward. As a result of the combined modulation by these three eddies, the BG freshwater extends directly southwestward from the river mouth to the central northern BoB and forms a long and narrow tongue-shaped plume.

In the second half of December 2015 (Fig. 8c), the SLA map clearly shows that a positive SLA extending from the bump of the IDM into the central BoB. Half a month later (Fig. 8d), the positive SLA signal strengthens and evolves into two continuous ACEs in the central BoB. A zonal Section S1 at 15.625°N is selected, which is approximately in the center of the two ACEs (Fig. 8c). The time-longitude plot of 20–120 d band-pass filtered SLA along Section S1 clearly indicates westward propagation with a phase

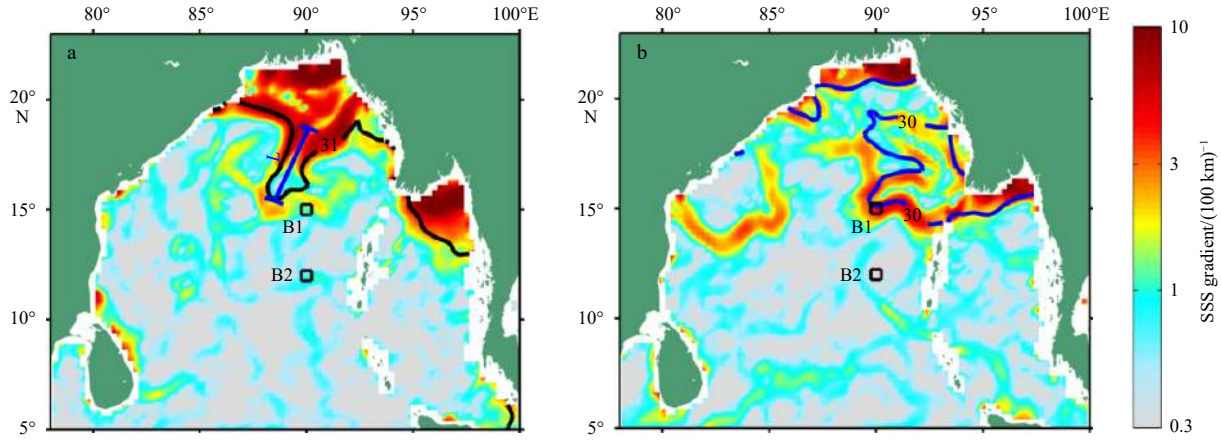

Fig. 7. The BG plume front on August 9, 2015 (a), and the Irrawaddy plume front on December 28, 2015 (b). The color indicates the gradient of SSS, and the black and blue lines represent the SSS contours of 31 and 30. The "L" indicates the length of the tongue shape of the BG plume front.

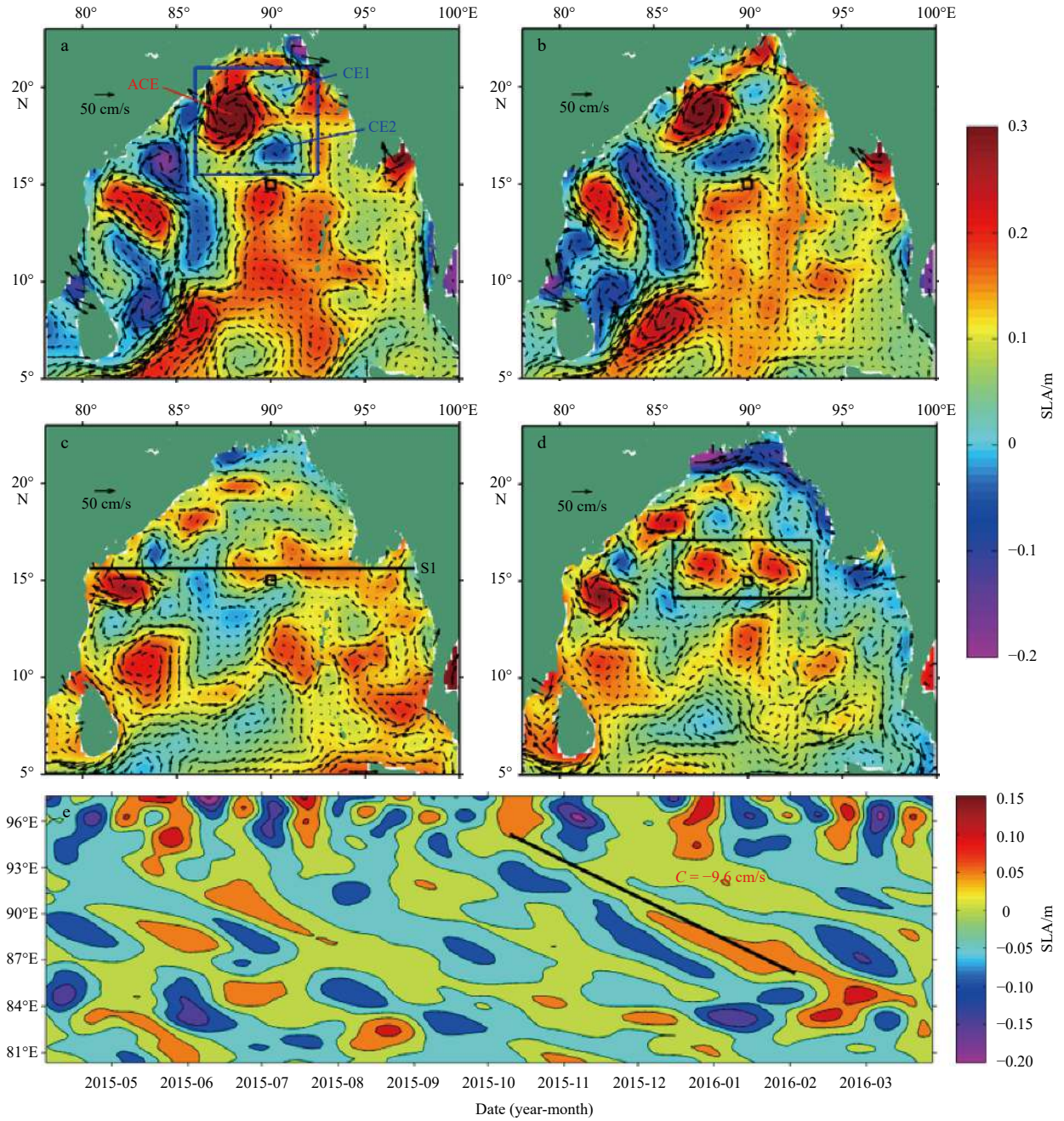

Fig. 8. CMEMS SLA (color) and associated geostrophic current (vectors) averaged over August 1–15, 2015 (a), August 16–31, 2015 (b), December 16–31, 2015 (c) and January 1–15, 2016 (d). The black rectangles highlight these eddies, and the bold black line indicates the Section S1 at 15.625°N. The black square represents the RAMA buoy at Station B1. Time-longitude plot of 20–120 day band-pass filtered SLA along Section S1 (e). ACE: anticyclonic eddy, CE1: cyclonic eddy 1, CE2: cyclonic eddy 2.

speed of –9.6 cm/s during the winter of 2015. These SLA maps (Figs 8c–e) indicate that two continuous ACEs propagating westward from the IDM modulate the Irrawaddy freshwater to extend into the central BoB.

Figure 9 shows the current vectors at Station B1 (15°N, 90°E) from the RAMA buoy (10 m layer, Fig. 9a), OSCAR (Fig. 9b) and CMEMS (geostrophic current associated with SLA, Fig. 9c) data. Although the RAMA buoy current data are not available from October 2015 to early March 2016, good agreements are still recognized among the three data. All of the current vectors clearly show strong intraseasonal variabilities due to the eddy activities. These eddy variabilities were also identified from the RAMA buoy current data at 15°N, 90°E by Girishkumar et al. (2017). These eddy activities and current variabilities can be interpreted by a combination of Figs 8 and 9 as follows.

The current vectors change direction from southeastward in the first half of August 2015 to northeastward in the second half of August 2015 (red lines in Fig. 9). This reflects that during this period, there is an ACE located in the south and a CE (CE2) located in the north and that the RAMA buoy Station B1 is located just between the two eddies (Fig. 8a). Therefore, the current vectors at Station B1 evolve with the evolution and propagation of

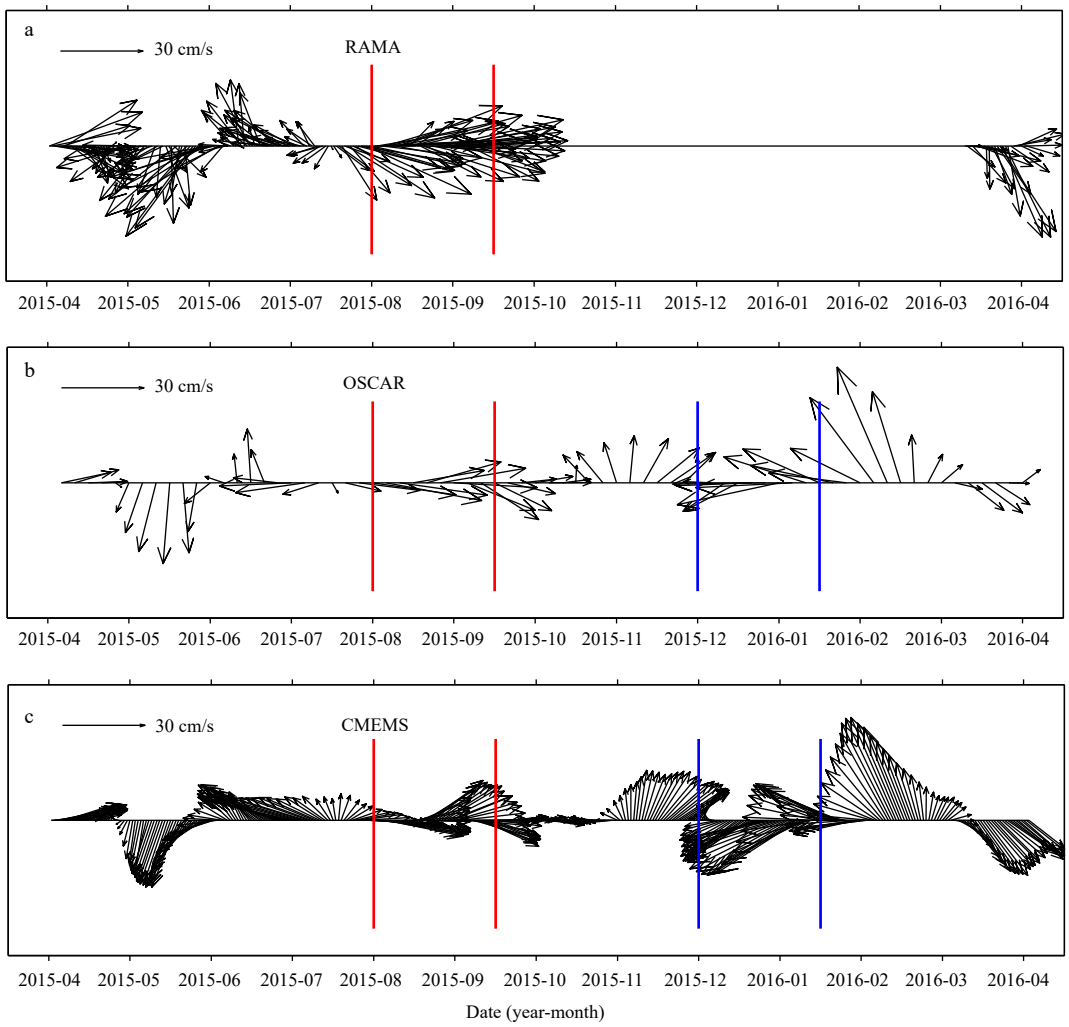

Fig. 9. Current vectors at Station B1 (15°N, 90°E) from the RAMA (a), OSCAR (b) and CMEMS (c, geostrophic current associated with SLA) data. Red and blue lines indicate summer and winter freshening, respectively.

the two eddies (Fig. 8b). Similarly, the current vectors change direction from southwestward in the second half of December 2015 to northwestward in the first half of January 2016 (blue lines in Fig. 9). This reflects that during this period, the positive SLA propagating westward into the central BoB evolves into an ACE (located in the west) and that the RAMA buoy Station B1 is located just in the southeast of the ACE (Fig. 8c). As with the evolution of the positive SLA, two ACEs are formed, and the RAMA buoy Station B1 is located just in the southwest of the second ACE (located in the east, Fig. 8d).

4 Discussion

The RAMA moored buoys along 90°E in the central BoB provide long-term, high quality upper oceanic data (McPhaden et al., 2009). Particularly, as the northernmost buoy station in the BoB, the RAMA buoy at 15°N, 90°E (B1, Fig. 1b) can well monitor the extension of BG and Irrawaddy freshwater. SMAP satellite provides a better SSS retrieval than the SMOS and Aquarius satellites, especially in coastal areas (Fournier et al., 2016, 2017), and thereby the data can well characterize the offshore extension of river freshwater in the northern BoB. The results show that SMAP SSS provides a good vision on how the river freshwater extends offshore from the river mouth and causes the freshening in the central northern BoB. It is confirmed that the freshening events observed from the RAMA moored buoy are directly due to the short-term offshore extension of the BG and Irrawaddy freshwater to the central northern BoB (Figs 3, 5 and 6). Sengupta et al. (2016) studied the pathways of the river freshwater in the northern BoB and concluded that the observed summer freshening pulse comes from the BG freshwater. However, because the Aquarius SSS has a data gap along the eastern boundary, the pathway of the Irrawaddy freshwater remains a source of speculation (Sengupta et al., 2016). Compared with the western part of the BoB, the eastern part is quite undersampled (Chatterjee et al., 2012; Akhil et al., 2014; Liu et al., 2018; Ashin et al., 2019). This leads to an unknown extension of the Irrawaddy freshwater, although its discharge is comparable to that of the BG River (Fig. 1c). These results provide direct evidences of the pathways of the offshore extension of the BG and Irrawaddy freshwater.

During summer, the BG freshwater extends offshore southwestward from the river mouth to the central northern BoB and forms a long and narrow tongue-shaped plume (Fig. 5). This long and narrow tongue-shaped plume may be the filament in the central BoB, which was suggested in several studies (Parampil et al., 2010; Benshila et al., 2014; Sree Lekha et al., 2018). Additionally, a strong salinity front is identified approximately along the

boundary of the BG freshwater plume in this study (Fig. 7). The tongue-shaped plume front is approximately 400 km long but has a narrow width. This long and narrow plume front may explain the large SSS gradient between two mooring stations in the central northern BoB (Sree Lekha et al., 2018). During winter, the Irrawaddy freshwater extends westward from the IDM into the central BoB (Fig. 6). Interestingly, when the Irrawaddy freshwater moves to the bump of the IDM, it bifurcates into two branches (Figs 6b–g). One branch continues extending westward to the central BoB and forms a tongue-shaped plume in the central BoB. This plume branch is responsible for the winter freshening observed by the RAMA buoy data (Fig. 6f). Another branch extends northward along the eastern BoB coast and then extends offshore to the central BoB. This study makes a difference from these recent studies that concerned the seasonal and interannual variability of freshwater extending along the BoB coast (Chatterjee et al., 2012; Akhil et al., 2014, 2016; Fournier et al., 2017). This study primarily aims to reveal the relationship between the frequently observed freshening events in the central BoB (Fig. 10) and the extension of river freshwater, and to further reveal the pathways of these river freshwater. These results provide direct evidences to demonstrate that the frequently observed freshening events are related to the short-term offshore extension of the BG and Irrawaddy freshwater, respectively.

Altimeter data show that the offshore extending freshwater plumes are the results of BG and Irrawaddy freshwater modulated by eddies. The BG freshwater is modulated by a combination of three eddies close to each other: a large ACE off the northwestern BoB coast and two CEs in the northern BoB (Figs 8a and b). The modulation of the BG freshwater by eddies along the western BoB was emphasized in recent studies (Sengupta et al., 2016; Fournier et al., 2017; Sree Lekha et al., 2018). The eddies in the northern BoB are reported chaotic and their formations are attributed to local monsoon wind and ocean internal variability (Babu et al., 2003; Kumar et al., 2007; Chen et al., 2012, 2018; Cheng et al., 2013, 2018). The formation mechanisms of the three eddies are not discussed here and more works need to be done in the future. The results in present study find that the Irrawaddy freshwater is modulated by two continuous ACEs (Figs 8c–e). The two ACEs are evolved from a positive SLA propagating westward from the bump of the IDM. The phase speed (9.6 cm/s) is very close to that of the downwelling Rossby wave in Yu and McPhaden (2011) and Cheng et al. (2018). Rossby waves propagating westward from the eastern boundary to the central BoB were attributed to local monsoon wind and remote forcing from the equator (Rao et al., 2010; Cheng et al., 2013, 2017; Suresh et al., 2013; Chen et al., 2017, 2018). The downwelling Rossby wave can converge the surface freshwater into the subsurface, this may explain why the RAMA buoy salinity shows a deeper winter freshening depth (Fig. 3a).

The freshwater plumes influence the upper ocean mixing and barrier layer formation in the BoB. Figure 11 shows the temporal evolution of daily temperature, potential density measured by the RAMA buoy at Station B1. In the upper ocean, the temperature is the warmest in spring, coldest in winter, and is relatively warmer in autumn and summer. The ILD is featured by a shallow ILD in spring and autumn, and a deep ILD in winter and summer. This reflects that the ILD is primarily controlled by the surface heat flux. The upper ocean density shows frequently very low surface density occurrences, which are caused by a high temperature (spring warming) or a low salinity (summer and winter freshening events). As a result, very shallow MLD (<10 m) is recognized during the period when the surface density is very low (Fig. 11b). Particularly, the thick ILD accompanied with a shallow MLD leading to a thick BLT, which is in particularly noticeable during the two freshening events.

5 Summary

The BoB receives a large amount of freshwater from the BG and the Irrawaddy rivers during the summer monsoon. These freshwater extends away from the river mouths and contributes to a strong near surface stratification, which influences the upper ocean mixing and air-sea interaction in the BoB (Han et al., 2001; Vinayachandran et al., 2002; Rao and Sivakumar, 2003; Thadathil et al., 2007; Akhil et al., 2016). In summer and winter of 2015, two significant freshening events with periods of weeks were observed from the RAMA moored buoy salinity. SMAP SSS compares well with the *in situ* data with a correlation of 0.88 and RMSD of 0.41. Based on the SMAP satellite observations, it is confirmed that the observed summer and winter freshening events are directly related to the short-term offshore extension of the BG and Irrawaddy freshwater, respectively. In summer, the BG freshwater is modulated by a combination of a large ACE and two CEs close to each other in the northern BoB. As a result, the freshwater extends southwestward from the river mouth to the central northern BoB and forms a long and narrow tongue-shaped plume. In winter, the Irrawaddy freshwater is modulated by two continuous ACEs evolved from Rossby wave propagating

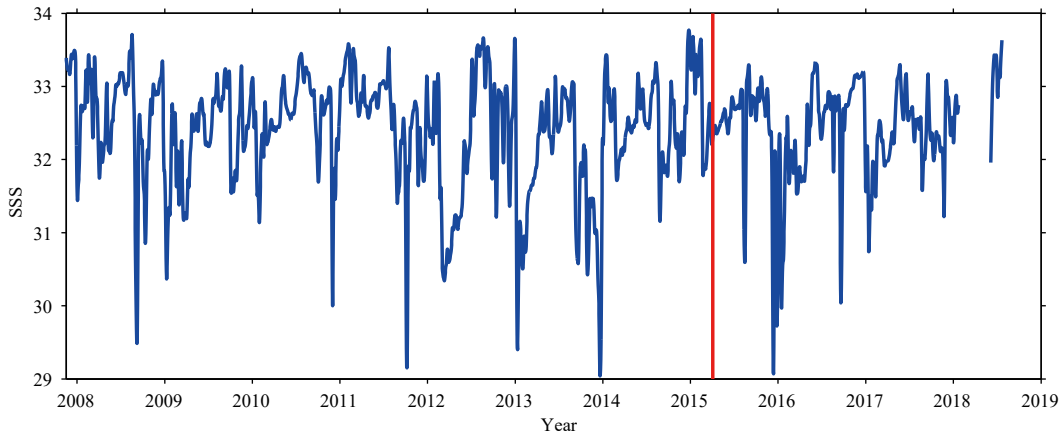

Fig. 10. Temporal evolution of daily SSS measured by the RAMA buoy salinity at Station B1 (15°N, 90°E) during 2007–2018. The red line indicates the starting period when the SMAP SSS data are available.

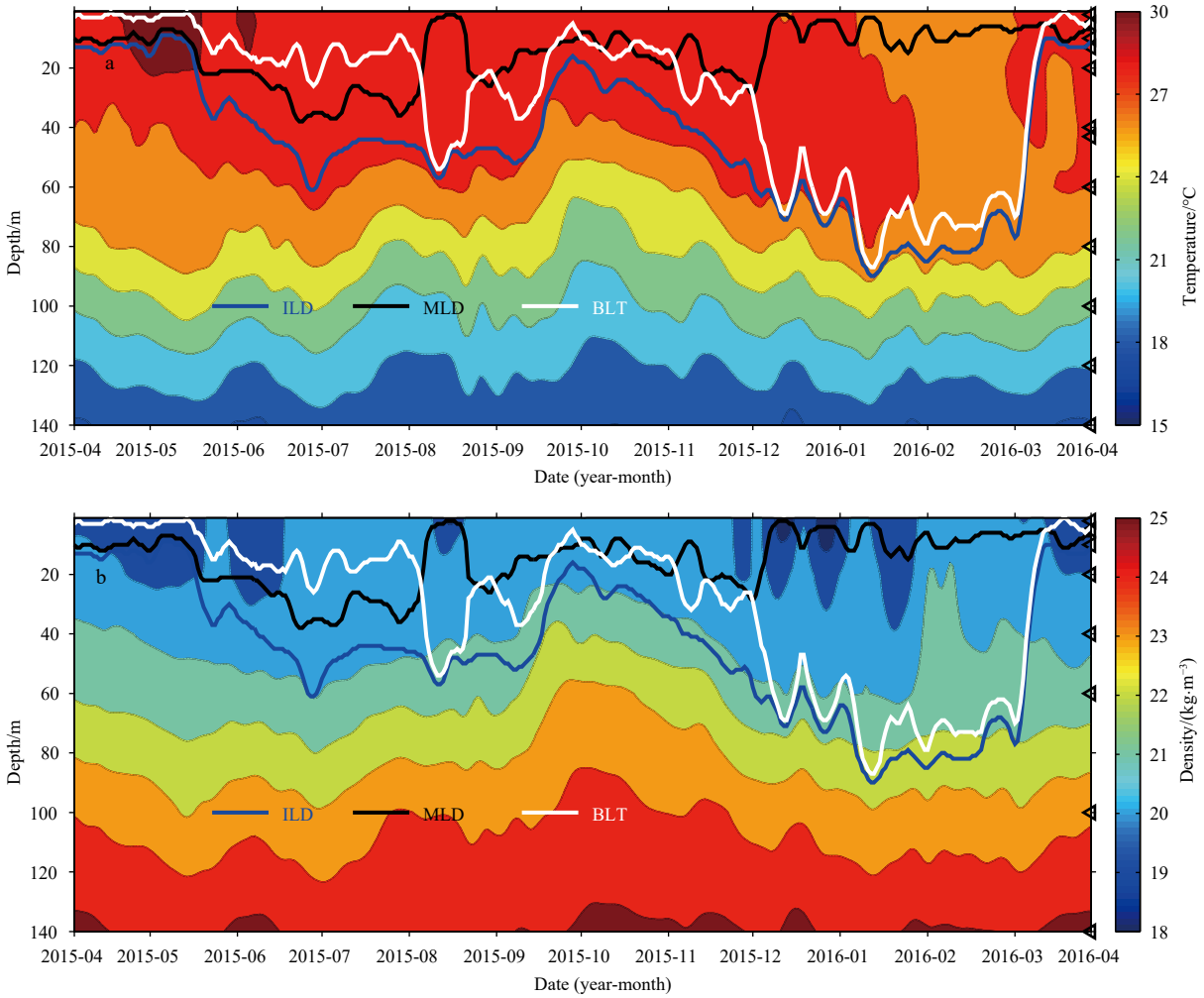

Fig. 11. Temporal evolution of 8 d smoothed daily temperature (a) and density (b) measured by the RAMA buoy at Station B1 (15°N, 90°E). The ILD (blue line), MLD (black line) and BLT (white line) are overlapped in the panels.

westward from the bump of the IDM. Therefore, the freshwater extends from the bump of the IDM into the central northern BoB. Strong plume fronts are formed along the boundaries of the BG and Irrawaddy freshwater plumes. This study provides direct evidences of the pathways of the offshore extension of BG and Irrawaddy freshwater to the central northern BoB and highlights the role of eddies in the freshwater plume variability.

References

Akhil V P, Durand F, Lengaigne M, et al. 2014. A modeling study of the processes of surface salinity seasonal cycle in the Bay of Bengal. Journal of Geophysical Research: Oceans, 119(6): 3926–3947, doi: 10.1002/2013JC009632

Akhil V P, Lengaigne M, Vialard J, et al. 2016. A modeling study of processes controlling the Bay of Bengal sea surface salinity interannual variability. Journal of Geophysical Research: Oceans, 121(12): 8471–8495, doi: 10.1002/2016JC011662

Arunraj K S, Jena B K, Suseentharan V, et al. 2018. Variability in eddy distribution associated with East India Coastal Current from high-frequency radar observations along southeast coast of India. Journal of Geophysical Research: Oceans, 123(12): 9101–9118, doi: 10.1029/2018JC014041

Ashin K, Girishkumar M S, Suprit K, et al. 2019. Observed upper ocean seasonal and intraseasonal variability in the Andaman Sea. Journal of Geophysical Research: Oceans, 124(10): 6760–6786, doi: 10.1029/2019JC014938

Babu M T, Kumar P S, Rao D P. 1991. A subsurface cyclonic eddy in the Bay of Bengal. Journal of Marine Research, 49(3): 403–410, doi: 10.1357/002224091784995846

Babu M T, Sarma Y V B, Murty V S N, et al. 2003. On the circulation in the Bay of Bengal during northern spring inter-monsoon (March–April 1987). Deep Sea Research Part II: Topical Studies in Oceanography, 50(5): 855–865, doi: 10.1016/S0967-0645(02)00609-4

Bao Senliang, Wang Huizan, Zhang Ren, et al. 2019. Comparison of satellite-derived sea surface salinity products from SMOS, Aquarius, and SMAP. Journal of Geophysical Research: Oceans, 124(3): 1932–1944, doi: 10.1029/2019JC014937

Benshila R, Durand F, Masson S, et al. 2014. The upper Bay of Bengal salinity structure in a high-resolution model. Ocean Modelling, 74: 36–52, doi: 10.1016/j.ocemod.2013.12.001

Bonjean F, Lagerloef G S E. 2002. Diagnostic model and analysis of the surface currents in the tropical Pacific Ocean. Journal of Physical Oceanography, 32(10): 2938–2954, doi: 10.1175/1520-0485(2002)032<2938:DMAAOT>2.0.CO;2

Chaitanya A V S, Lengaigne M, Vialard J, et al. 2014. Salinity measurements collected by fishermen reveal a "river in the sea" flowing along the Eastern Coast of India. Bulletin of the American Meteorological Society, 95(12): 1897–1908, doi: 10.1175/BAMS-D-12-00243.1

Chatterjee A, Shankar D, Shenoi S S C, et al. 2012. A new atlas of temperature and salinity for the north Indian Ocean. Journal of Earth System Science, 121(3): 559–593, doi: 10.1007/s12040-

012-0191-9
Chen Gengxin, Han Weiqing, Li Yuanlong, et al. 2017. Strong intraseasonal variability of meridional currents near 5°N in the Eastern Indian Ocean: Characteristics and causes. Journal of Physical Oceanography, 47(5): 979–998, doi: 10.1175/JPO-D-16-0250.1
Chen Gengxin, Li Yuanlong, Xie Qiang, et al. 2018. Origins of eddy kinetic energy in the Bay of Bengal. Journal of Geophysical Research: Oceans, 123(3): 2097–2115, doi: 10.1002/2017JC013455
Chen Gengxin, Wang Dongxiao, Hou Yijun. 2012. The features and interannual variability mechanism of mesoscale eddies in the Bay of Bengal. Continental Shelf Research, 47: 178–185, doi: 10.1016/j.csr.2012.07.011
Cheng Xuhua, McCreary J P, Qiu Bo, et al. 2017. Intraseasonal-to-semiannual variability of sea-surface height in the astern, equatorial Indian Ocean and southern Bay of Bengal. Journal of Geophysical Research: Oceans, 122(5): 4051–4067, doi: 10.1002/2016JC012662
Cheng Xuhua, McCreary J P, Qiu Bo, et al. 2018. Dynamics of eddy generation in the central Bay of Bengal. Journal of Geophysical Research: Oceans, 123(9): 6861–6875, doi: 10.1029/2018JC014100
Cheng Xuhua, Xie Shangping, McCreary J P, et al. 2013. Intraseasonal variability of sea surface height in the Bay of Bengal. Journal of Geophysical Research: Oceans, 118(2): 816–830, doi: 10.1002/jgrc.20075
da Silva C E, Castelao R M. 2018. Mississippi River plume variability in the Gulf of Mexico from SMAP and MODIS-Aqua observations. Journal of Geophysical Research: Oceans, 123(9): 6620–6638, doi: 10.1029/2018JC014159
Dai Aiguo, Qian Taotao, Trenberth K E, et al. 2009. Changes in continental freshwater discharge from 1948 to 2004. Journal of Climate, 22(10): 2773–2792, doi: 10.1175/2008JCLI2592.1
Das B K, Anandh T S, Kuttippurath J, et al. 2019. Characteristics of the discontinuity of western boundary current in the Bay of Bengal. Journal of Geophysical Research: Oceans, 124(7): 4464–4479, doi: 10.1029/2019JC015235
Du Yan, Xie Shangping, Huang Gang, et al. 2009. Role of air-sea interaction in the long persistence of El Niño-induced North Indian Ocean warming. Journal of Climate, 22(8): 2023–2038, doi: 10.1175/2008JCLI2590.1
Felton C S, Subrahmanyam B, Murty V S N, et al. 2014. Estimation of the barrier layer thickness in the Indian Ocean using Aquarius Salinity. Journal of Geophysical Research: Oceans, 119(7): 4200–4213, doi: 10.1002/2013JC009759
Fore A G, Yueh S H, Tang Wenqing, et al. 2016. Combined active/passive retrievals of ocean vector wind and sea surface salinity with SMAP. IEEE Transactions on Geoscience & Remote Sensing, 54(12): 7396–7404
Fournier S, Reager J T, Lee T, et al. 2016. SMAP observes flooding from land to sea: The Texas event of 2015. Geophysical Research Letters, 43(19): 10338–10346, doi: 10.1002/2016GL070821
Fournier S, Vialard J, Lengaigne M, et al. 2017. Modulation of the Ganges-Brahmaputra river plume by the Indian Ocean dipole and eddies inferred from satellite observations. Journal of Geophysical Research: Oceans, 122(12): 9591–9604, doi: 10.1002/2017JC013333
Girishkumar M S, Joseph J, Thangaprakash V P, et al. 2017. Mixed layer temperature budget for the northward propagating Summer Monsoon Intraseasonal Oscillation (MISO) in the Central Bay of Bengal. Journal of Geophysical Research: Oceans, 122(11): 8841–8854, doi: 10.1002/2017JC013073
Hackert E C, Kovach R M, Busalacchi A J, et al. 2019. Impact of Aquarius and SMAP satellite sea surface salinity observations on coupled El Niño/Southern Oscillation forecasts. Journal of Geophysical Research: Oceans, 124(7): 4546–4556, doi: 10.1029/2019JC015130
Han Weiqing, McCreary J P Jr. 2001. Modeling salinity distributions in the Indian Ocean. Journal of Geophysical Research, 106(C1): 859–877, doi: 10.1029/2000JC000316
Han Weiqing, McCreary J P Jr, Kohler K E. 2001. Influence of precipitation minus evaporation and Bay of Bengal rivers on dynamics, thermodynamics, and mixed layer physics in the upper Indian Ocean. Journal of Geophysical Research, 106(C4): 6895–6916, doi: 10.1029/2000JC000403
Hosoda S, Ohira T, Nakamura T. 2008. A monthly mean dataset of global oceanic temperature and salinity derived from Argo float observations. JAMSTEC Report of Research and Development, 8: 47–59, doi: 10.5918/jamstecr.8.47
Kara A B, Rochford P A, Hurlburt H E. 2000. An optimal definition for ocean mixed layer depth. Journal of Geophysical Research, 105(C7): 16803–16821, doi: 10.1029/2000JC900072
Kumar P S, Nuncio M, Ramaiah N, et al. 2007. Eddy-mediated biological productivity in the Bay of Bengal during fall and spring intermonsoons. Deep Sea Research Part I: Oceanographic Research Papers, 54(9): 1619–1640, doi: 10.1016/j.dsr.2007.06.002
Le Vine D M, Dinnat E P, Meissner T, et al. 2018. Status of Aquarius and salinity continuity. Remote Sensing, 10(10): 1585, doi: 10.3390/rs10101585
Li Yuanlong, Han Weiqing, Ravichandran M, et al. 2017a. Bay of Bengal salinity stratification and Indian summer monsoon intraseasonal oscillation: 1. Intraseasonal variability and causes. Journal of Geophysical Research: Oceans, 122(5): 4291–4311, doi: 10.1002/2017JC012691
Li Yuanlong, Han Weiqing, Wang Wanqiu, et al. 2016. Intraseasonal variability of SST and precipitation in the Arabian Sea during the Indian summer monsoon: Impact of ocean mixed layer depth. Journal of Climate, 29(21): 7889–7910, doi: 10.1175/JCLI-D-16-0238.1
Li Yuanlong, Han Weiqing, Wang Wanqiu, et al. 2017b. Bay of Bengal salinity stratification and Indian summer monsoon intraseasonal oscillation: 2. Impact on SST and convection. Journal of Geophysical Research: Oceans, 122(5): 4312–4328, doi: 10.1002/2017JC012692
Li Yuanlong, Han Weiqing, Wang Wanqiu, et al. 2018. The Indian summer monsoon intraseasonal oscillations in CFSv2 forecasts: Biases and importance of improving air-sea interaction processes. Journal of Climate, 31(14): 5351–5370, doi: 10.1175/JCLI-D-17-0623.1
Liu Yanliang, Li Kuiping, Ning Chunlin, et al. 2018. Observed seasonal variations of the upper ocean structure and air-sea interactions in the Andaman Sea. Journal of Geophysical Research: Oceans, 123(2): 922–938, doi: 10.1002/2017JC013367
Liu Lin, Yu Weidong, Li T. 2011. Dynamic and thermodynamic air-sea coupling associated with the Indian Ocean dipole diagnosed from 23 WCRP CMIP3 models. Journal of Climate, 24(18): 4941–4958, doi: 10.1175/2011JCLI4041.1
McCreary J P Jr, Kundu P K, Molinari R L. 1993. A numerical investigation of dynamics, thermodynamics and mixed-layer processes in the Indian Ocean. Progress in Oceanography, 31(3): 181–244, doi: 10.1016/0079-6611(93)90002-U
McPhaden M J, Meyers G, Ando K, et al. 2009. RAMA: The research moored array for African-Asian-Australian monsoon analysis and prediction. Bulletin of the American Meteorological Society, 90(4): 459–480, doi: 10.1175/2008BAMS2608.1
Melnichenko O, Hacker P, Maximenko N, et al. 2014. Spatial optimal interpolation of *Aquarius* sea surface salinity: algorithms and implementation in the North Atlantic. Journal of Atmospheric and Oceanic Technology, 31(7): 1583–1600, doi: 10.1175/JTECH-D-13-00241.1
Murty V S N, Sarma Y V B, Rao D P, et al. 1992. Water characteristics, mixing and circulation in the Bay of Bengal during southwest monsoon. Journal of Marine Research, 50(2): 207–228, doi: 10.1357/002224092784797700
Papa F, Bala S K, Pandey R K, et al. 2012. Ganga-Brahmaputra river discharge from Jason-2 radar altimetry: An update to the long-term satellite-derived estimates of continental freshwater forcing flux into the Bay of Bengal. Journal of Geophysical Research, 117: C11021
Papa F, Durand F, Rossow W B, et al. 2010. Satellite altimeter-derived monthly discharge of the Ganga-Brahmaputra River and its

seasonal to interannual variations from 1993 to 2008. Journal of Geophysical Research, 115: C12013, doi: 10.1029/2009JC006075

Parampil S R, Gera A, Ravichandran M, et al. 2010. Intraseasonal response of mixed layer temperature and salinity in the Bay of Bengal to heat and freshwater flux. Journal of Geophysical Research, 115: C05002

Qiu Yun, Cai Wenjun, Li Li, et al. 2012. Argo profiles variability of barrier layer in the tropical Indian Ocean and its relationship with the Indian Ocean Dipole. Geophysical Research Letter, 39: L08605

Rao R R, Kumar M S G, Ravichandran M, et al. 2010. Interannual variability of Kelvin wave propagation in the wave guides of the equatorial Indian Ocean, the coastal Bay of Bengal and the southeastern Arabian Sea during 1993–2006. Deep Sea Research Part I: Oceanographic Research Papers, 57(1): 1–13, doi: 10.1016/j.dsr.2009.10.008

Rao S A, Saha S K, Pokhrel S, et al. 2011. Modulation of SST, SSS over northern Bay of Bengal on ISO time scale. Journal of Geophysical Research, 116: C09026

Rao R R, Sivakumar R. 2003. Seasonal variability of sea surface salinity and salt budget of the mixed layer of the north Indian Ocean. Journal of Geophysical Research, 108(C1): 3009, doi: 10.1029/2001JC000907

Sengupta D, Bharath Raj G N, Ravichandran M, et al. 2016. Near-surface salinity and stratification in the north Bay of Bengal from moored observations. Geophysical Research Letters, 43(9): 4448–4456, doi: 10.1002/2016GL068339

Sengupta D, Bharath Raj G N, Shenoi S S C. 2006. Surface freshwater from Bay of Bengal runoff and Indonesian throughflow in the tropical Indian Ocean. Geophysical Research Letters, 33: L22609, doi: 10.1029/2006GL027573

Shetye S R, Gouveia A D, Shankar D, et al. 1996. Hydrography and circulation in the western Bay of Bengal during the northeast monsoon. Journal of Geophysical Research, 101(C6): 14011–14025, doi: 10.1029/95JC03307

Shetye S R, Shenoi S S C, Gouveia A D, et al. 1991. Wind-driven coastal upwelling along the western boundary of the Bay of Bengal during the southwest monsoon. Continental Shelf Research, 11(11): 1397–1408, doi: 10.1016/0278-4343(91)90042-5

Sprintall J, Tomczak M. 1992. Evidence of the barrier layer in the surface layer of the tropics. Journal of Geophysical Research, 97(C5): 7305–7316, doi: 10.1029/92JC00407

Sree Lekha J, Buckley J M, Tandon A, et al. 2018. Subseasonal dispersal of freshwater in the northern Bay of Bengal in the 2013 summer monsoon season. Journal of Geophysical Research: Oceans, 123(9): 6330–6348, doi: 10.1029/2018JC014181

Sun Qiwei, Du Yan, Zhang Yuhong, et al. 2019. Evolution of sea surface salinity anomalies in the southwestern tropical Indian Ocean during 2010–2011 influenced by a negative IOD event. Journal of Geophysical Research: Oceans, 124(5): 3428–3445, doi: 10.1029/2018JC014580

Suresh I, Vialard J, Lengaigne M, et al. 2013. Origins of wind-driven intraseasonal sea level variations in the North Indian Ocean coastal waveguide. Geophysical Research Letters, 40(21): 5740–5744, doi: 10.1002/2013GL058312

Tang Wenqing, Fore A, Yueh S, et al. 2017. Validating SMAP SSS with in situ measurements. Remote Sensing of Environment, 200: 326–340, doi: 10.1016/j.rse.2017.08.021

Thadathil P, Muraleedharan P M, Rao R R, et al. 2007. Observed seasonal variability of barrier layer in the Bay of Bengal. Journal of Geophysical Research, 112: C02009

Thadathil P, Suresh I, Gautham S, et al. 2016. Surface layer temperature inversion in the Bay of Bengal: Main characteristics and related mechanisms. Journal of Geophysical Research: Oceans, 121(8): 5682–5696, doi: 10.1002/2016JC011674

Thangaprakash V P, Girishkumar M S, Suprit K, et al. 2016. What controls seasonal evolution of sea surface temperature in the Bay of Bengal? Mixed layer heat budget analysis using moored buoy observations along 90°E. Oceanography, 29(2): 202–213, doi: 10.5670/oceanog.2016.52

Vinayachandran P N, Murty V S N, Ramesh Babu V. 2002. Observations of barrier layer formation in the Bay of Bengal during summer monsoon. Journal of Geophysical Research, 107(C12): 8018

Xi Jingyuan, Zhou Lei, Murtugudde R, et al. 2015. Impacts of intraseasonal SST anomalies on precipitation during Indian summer monsoon. Journal of Climate, 28(11): 4561–4575, doi: 10.1175/JCLI-D-14-00096.1

Yu Lisan, McPhaden M J. 2011. Ocean preconditioning of Cyclone Nargis in the Bay of Bengal: interaction between Rossby waves, surface fresh waters, and sea surface temperatures. Journal of Physical Oceanography, 41(9): 1741–1755, doi: 10.1175/2011JPO4437.1

Zhou Lei, Murtugudde R. 2014. Impact of northward-propagating intraseasonal variability on the onset of Indian summer monsoon. Journal of Climate, 27(1): 126–139, doi: 10.1175/JCLI-D-13-00214.1